Engineering Band Structure via the Site Preference of Pb^{2+} in the In^{+} Site for Enhanced Thermoelectric Performance of In_6Se_7

Jiaolin Cui,[1*] Min Cheng,[1,2] Wenchang Wu,[1] Zhengliang Du,[1] Yimin Chao[3*]
1– School of Materials & Chemical Engineering, Ningbo University of Technology, Ningbo, 315016, China
2–Materials Science and Engineering College, Taiyuan University of Technology, Taiyuan, 030024, China
3–School of Chemistry, University of East Anglia, Norwich NR4 7TJ, United Kingdom

ABSTRACT Although binary In-Se based alloys as thermoelectric (TE) candidates are of interests in recent years, little attention has been paid into In_6Se_7 based compounds. With substituting Pb in In_6Se_7, the preference of Pb^{2+} in the In^{+} site has been observed, allowing the Fermi level (F_r) shift towards the conduction band and the localized state conduction becomes dominated. Consequently, the Hall carrier concentration (n_H) has been enhanced significantly with the highest n_H value being about 2~3 orders of magnitude higher than that of Pb-free sample. Meanwhile, the lattice thermal conductivity (κ_L) tends to be reduced as n_H value increases, owing to an increased phonon scattering on carriers. As a result, a significantly enhanced TE performance has been achieved with the highest TE figure of merit (ZT) of 0.4 at ~850 K. This ZT value is 27 times that of intrinsic In_6Se_7 (ZT=0.015 at 640 K), which proves a successful band structure engineering through site preference of Pb in In_6Se_7.
Keywords: Thermoelectric performance; Band structure engineering; Site preference; In_6Se_7; Fermi Level; Carrier concentration

1. Introduction

Thermoelectric (TE) devices are capable of converting heat into electricity or vice versa for power generation or cooling without moving mechanical parts, therefore, they have attracted much attention in industry. However, bulk materials, which can be effectively used in TE devices, are still limited so far. A remarkable improvement in TE performance is still a critical challenge owing to the inverse dependence of Seebeck coefficient (α) and electrical conductivity (σ) on carrier concentration (n). These parameters directly govern the TE figure of merit (ZT):

$$ZT=T\alpha^2\sigma/\kappa= T\alpha^2\sigma/(\kappa_L+\kappa_e) \quad (1)$$

where, κ is the total thermal conductivity, while the κ_L, κ_e are the lattice and electronic contribution, respectively.

In order to enhance the ZT value, many new materials have been developed in recent years, such as, copper chalcogenide Cu_2Se,[1] SnSe-[2,3] and In_4Se_3-based crystals.[4-7]

Owing to their unique intrinsic structures, such as phases, crystal structures, and structural imperfection,[8] binary In-Se based compounds possess potential in TE performances. For example, the In_4Se_3-based alloys give ZT=1.48 @ 705 K,[4] and 1.11 @ 723 K,[7] and the In_2Se_3-based alloy ZT=1.23 @ 916 K).[9] However, among the In-Se based compounds the InSe- or In_6Se_7-based alloys as TE candidates have not been paid much attention yet.[8]

Walther etc. determined that that In_6Se_7 crystallizes in a monoclinic crystal structure (space group: $P2_1/m$), where indium presents multiple valences (1+, 2+ and 3+).[10-12] Hence the compound In_6Se_7 can be formally described as $In^{+}[In_2]^{4+}(In^{3+})_3(Se^{2-})_7$ presuming that the oxidation state of Se is 2-,[10-12] where the $[In_2]^{4+}$ and In^{3+} ions occupy two and three different sites respectively. The crystal structure of In_6Se_7 is shown in Figure S1 as Supporting Information. Recent investigations on In_6Se_7 revealed p to n-type transition when Sn is incorporated and that the TE performance has been improved. Such an improvement is related to the creation of the defect Sn_{In}^{3+} acting as a donor, since Sn^{4+} is energetically favorable to In^{+} site. Nevertheless, the improvement is limited because of the negative effect of Sn^{2+}, which prefers the In^{3+} site,

* Corresponding authors: cuijiaolin@163.com; Y.Chao@uea.ac.uk

neutralizing the effect of Sn^{4+}.[13] In addition, there are some deep impurity levels formed if Sn occupies the $[In_2]^{4+}$ and In^{3+} sites. These impurity levels act as annihilation centres for electrons and holes, thus making a negative contribution to the carrier concentration.[13]

Although Sn and Pb lie in the same column in the periodic table, the behavior of Pb is quite different from that of Sn in In-Se compounds. For instance, Sn acts as a donor in InSe while Pb is an acceptor.[14] In addition, the element Sn in InSe or In_6Se_7 can create some deep impurity levels, and it is hard to alter the large charged defect concentration in the forbidden gap.[13, 15] Since an incorporation of Pb in chalcogenide glasses In-Se could unpin the Fermi level (F_r),[16] it allows the F_r shift toward the conduction band, and enables the conductivity of Pb doped samples to be several orders of magnitude larger than the undoped In-Se samples.[16]

In this study, samples of substituting Pb for In in In_6Se_7 have been prepared, and their structures and transport properties have been examined. It has been observed that the unpinning of the Fermi level induced by the site preference of Pb^{2+} in the In^+ site, effectively engineers the band structures and significantly improves the TE performance.

2. EXPERIMENTAL SECTION

Three elements In, Pb, and Se with a purity of 99.999% were loaded in different vacuum silica tubes, according to the formula $In_{6-x}Pb_xSe_7$ (x=0, 0.1, 0.3, 0.5, 0.7), and then melted at 1273 K for 24 h. The detailed preparation methods of the materials are similar to those reported in the previous publications.[13,17,18]

The Hall coefficients (R_H) were measured on a Physical Property Measurement System (PPMS) using the Van der Pauw method in a magnetic field up to ±1.5 T at room temperature (RT) and 390 K. The Hall mobility (μ) and carrier concentrations (n_H) were subsequently calculated based on the relations $\mu=|R_H|\sigma$ and $n_H=1/(R_He)$, where e is the electron charge.

The Seebeck coefficients (α) and electrical conductivities (σ) were measured using an ULVAC ZEM-3 under a helium atmosphere in the range from RT and ~850 K. The uncertainty of each measurement is about 6%. The thermal conductivities (κ) were calculated from $\kappa=dC_p\lambda$ with the diffusivity (λ) measured by the TC-1200RH at RT~850 K (uncertainty < 10%). The heat capacities (C_p) were estimated using Dulong–Petit rule, and d is the material density. The lattice contributions (κ_L) were attained from the total κ minus the electronic part κ_e. κ_e is estimated by Wiedemann–Franz (W-F) relation, $\kappa_e = L_0\sigma T$, where the L_0 is the Lorenz constant estimated to be 2.2×10^{-8} $W\Omega K^{-2}$.[19] The data obtained was repeated for several times using different samples. The total uncertainty for ZT was ~18%.

Similar experimental procedures, including the preparation of the samples, compositional (EDAX) analyses, XPS spectra analyses, and the measurement details of the physical parameters (α, σ,etc.) have been used here as in the previous works.[13,17,18] The density of states (DOS) and the formation energy (E_f) have been calculated as in the previous publication, see reference [13].

3. RESULTS AND DISCUSSION

3.1. Chemical compositions and structures

The back-scattered SEM images for the $In_{6-x}Pb_xSe_7$ (x=0.3) bulk sample are shown in Figure S2 as Supporting Information, while the mapping images and the EDAX spectrum are displayed in Figure S3. There is no visible textured structure observed from the dense samples (more than 98.0% theoretical density 6.21 $g.cm^{-3}$),[11] either parallel or perpendicular to the pressing direction, see Figure S2. Therefore, we did not measure the transport properties in different pressing directions, according to the previous experience.[20] The average chemical compositions of the sample (x=0.3) were determined by a mapping of EPMA, revealing a slight Se deficiency and In excess. The detailed chemical compositions are presented in Table S1 as

Supporting Information, where the Se molars are normalized to 7. Generally, the identified relative molars of In, Pb and Se are close to nominal ones, which suggest that the compositions within the final samples are almost as intended.

XRD analysis shows that materials exhibit monoclinic In_6Se_7-based solid solution (space group: $P2_1/m$, PDF:85-0184) in all the composition range (x=0~0.7), as shown in Figure S4 as Supporting Information. Interestingly, both the lattice constants a and c increase linearly with Pb content increasing (see Figure 1), whereas the b value keeps almost the same (4.056 Å). The data from Welther[10] and Deeb[12] are plotted in Figure 1 for comparison. The gradual increase of the lattice constants a and c is likely due to the decreased attraction between cation and anion Se, because Pb (2.33) has much higher electronegativity than In (1.78). Furthermore, the linear relationship between the lattice constants and Pb content, which follows the Vegard's law, suggests the element Pb has been incorporated into the In_6Se_7 lattices, either substutionally or interstitially, since there are interstitial In atoms in In_6Se_7.[21]

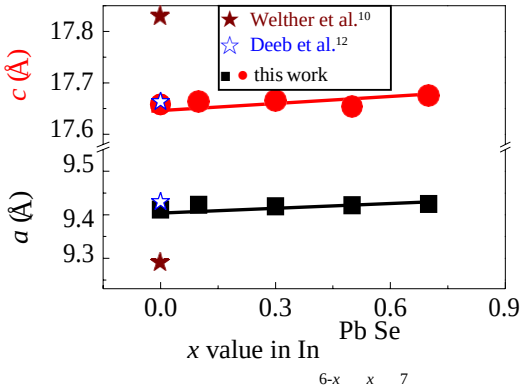

Figure 1. Lattice constants a and c as a function of Pb content.

In order to determine the valence charges of Pb in the lattice of $In_{6-x}Pb_xSe_7$, XPS spectra are employed to investigate the oxidation states. XPS spectra in the region of Pb4$f_{7/2}$ at x=0.1~0.7 are shown in Figure S5. The XPS binding energies of Pb4$f_{7/2}$ (uncertainty: ~±0.01 eV) are around 137.67~138.15 eV, which confirms the presence of Pb^{2+}.[22-25] While those of In and Se elements take the usual oxidation states as those in the Sn-substituted In_6Se_7,[13] see Table S2.

In order to determine the site preference of Pb^{2+} in In_6Se_7, it is necessary to calculate the density of states (DOS) and formation energies (E_f) upon Pb-incorporation at different In sites using first principle calculation, as shown in Figure 2. The DOS of intrinsic In_6Se_7 is reported in the previous publication, see reference [13] and shown in Figure S6 as Supporting Information, where the Fermi level (F_r) is just above the valence band maximum (VBM). Upon Pb^{2+} occupation in $In^{3+}(1)$, $In^{3+}(2)$ or $In^{3+}(3)$ site, the formation energy (E_f) is -0.33 ~ -0.40 eV, and F_r moves into the valence band. The bandgap (E_g) reduces from 0.86 eV (x=0) to 0.31~0.35 eV (Figure 2a-c). If Pb^{2+} occupies the $In^{2+}(1)$ or $In^{2+}(2)$ site, F_r lies in the middle of bandgap or valence band. E_f value is -0.39~ -0.40 eV, as shown in Figure 2d,e. It is worth noting that F_r shifts into the conduction band with E_f = -0.82 eV as Pb^{2+} occupies the In^+ site, which is the lowest formation energy among different Pb^{2+} occupations (Figure 2f). Therefore, it is reasonable to suggest that Pb^{2+} prefers the In^+ to In^{3+} site, which creates donor defect Pb_{In}^+. However, it is difficult to rule out the possibility that some Pb^{2+} occupies the In^{2+} site when Pb content (x) exceeds a certain critical value in the matrix.

If Pb^{2+} is energetically favorable to the In^+ site, the chemical/crystal environment should be described as below:

$$In_{6-j}\ Pb_j\ e_jSe_7 \qquad \text{(upon divalent } Pb^{2+} \text{ occupation in } In^+ \text{ site)} \qquad (2)$$

where e_j *is* the created extra electrons. However, there should have no extra electrons or holes created if Pb^{2+} occupies the In^{2+} sites, in the light of the chemical environment.

3.2. Carrier concentrations

In order to verify the contribution of site preference of Pb^{2+} to the carrier concentration, the Hall

coefficients (R_H) have been measured at RT and 390 K, and the Hall carrier concentrations (n_H) and mobility (μ) have been calculated as a function of Pb content x, as shown in Figure 3a. The Pb-free sample exhibits p-type semiconducting behavior, because the R_H values are positive, while the Pb-incorporated samples are n-type. From Figure 3a it is observed that the n_H value increases as Pb content increases before it turns to decrease at x=0.5. At x=0.5 the n_H values, 2.39×10^{25} m^{-3} at RT and 9.79×10^{25} m^{-3} at 390 K, are near the optimal concentration in thermoelectrics,[26] which are about 2~3 orders of magnitude higher than that of Pb-free sample. The composition dependent mobility (μ) at RT is analogous to n_H. The mobility reaches the highest value (7.30 $m^2v^{-1}s^{-1}$) at x=0.5, which is about 2 times that of Pb-free sample. However, the mobility at 390 K reveals decreasing tendency as x value increases up to x=0.3~0.4.

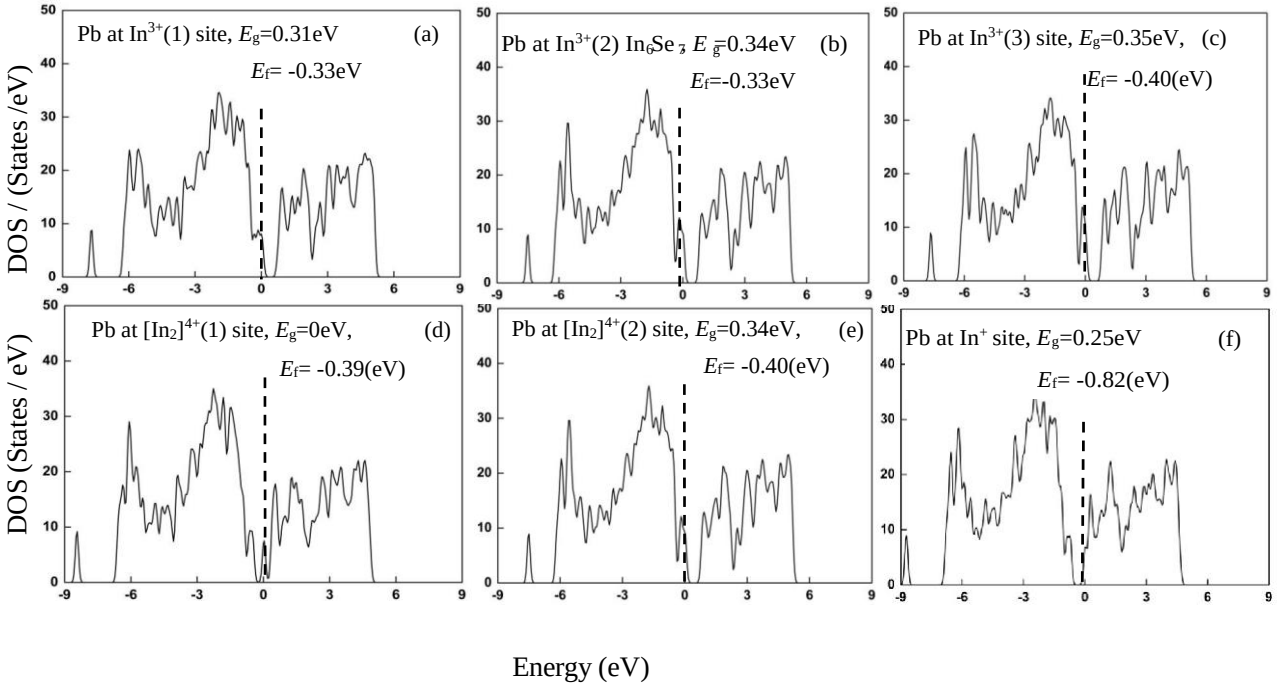

Figure 2. The DOS and E_f upon Pb-incorporation: (a) Pb at In^{3+}(1) site, E_f= -0.33eV; (b) Pb at In^{3+}(2) site, E_f= -0.33eV; (c) Pb at In^{3+}(3) site, E_f= -0.40eV; (d) Pb at $[In_2]^{4+}$(1) site, E_f= -0.39eV; (e) Pb at $[In_2]^{4+}$(2) site, E_f= -0.40eV; (f) Pb at In^+ site, E_f= -0.82eV.

Assuming that the chemical control over carrier density in In_6Se_7 can be achieved simply by element substitution, and the carrier density in Pb-substituted In_6Se_7 estimated using the valence counting rule,[27-29] the theoretical carrier densities ($n_{cal.}$), $n_{cal.}=n_{max}(1-j)$, based on the description (2), using $n_{max}\approx8.99\times10^{22}$ m^{-3} corresponding to intrinsic In_6Se_7 (p-type) at RT,[13] are calculated and shown in Figure 3b. Surprisingly, there is no agreement between the measured Hall carrier concentrations n_H and calculated n_{cal} values. The n_H values at RT are about 2 orders of magnitude higher than the calculated n_{cal}, which indicates that the measured carrier density in the present materials do not follow the valence counting rule.

3.3 Thermoelectric transport properties

The Seebeck coefficients (α) as a function of temperature are displayed in Figure 4a, and an insert is the close-up view of α values for Pb-incorporated samples. The α values for the Pb-free sample are positive below 835 K, and above that the α value turns to negative. Meanwhile, those for the Pb-incorporated ones are negative over the entire temperature range, suggesting a complete transition from p to n type. Such a transition has also been observed in many chalcogenides, such as Bi-doped Ge-Se or Ge-Te-Se,[30,31]

Pb-doped Ge-Se glasses,[16,32] Se-In compounds,[33] which is ascribed to the disturbance of the equilibrium between the charged defect states of Se–In glass owing to the formation of ionic Pb^{2+}-Se^{2-} bonds.[16] In addition, the absolute α value at lower temperatures generally decreases with Pb content increasing, and the maximum $|\alpha|$ values appear around 730 K, from 288.59 μVK^{-1} at x=0.1 to 178.14 μVK^{-1} at x=0.7 as Pb content increases, see the insert in Figure 4a. The decrease of the $|\alpha|$ value is likely resulted from the enhancement of carrier concentration n_H (Figure 3a). Figure 4b is the plot of electrical conductivities (σ) against temperature, where the σ value roughly increases with Pb content and temperature increasing with the maximum values appear at 835~840 K. The highest σ values are 7.24×10^3 $\Omega^{-1}m^{-1}$ for x=0.5 and 8.03×10^3 $\Omega^{-1}m^{-1}$ for x=0.7 at 835~840 K. However, the σ value for Pb-free sample increases with temperature monotonically.

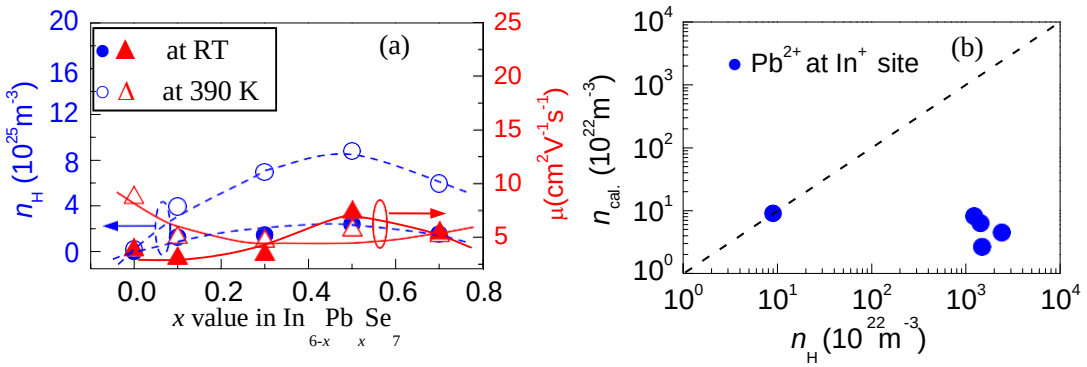

Figure 3. (a) Measured Hall carrier concentration (n_H) and mobility (μ) against x value in $In_{6-x}Pb_xSe_7$. (b) Calculated theoretical carrier densities ($n_{cal.}$) against Hall concentration (n_H).

Figure 4c shows the temperature dependence of the lattice thermal conductivity (κ_L), and the total κ values are shown as an insert. The lower left inset is the close-up view of κ_L at high temperatures, which clearly indicates that κ_L reduces with Pb content increasing. However, the κ_L value at ~850 K seems to convergence at $x \geq 0.5$ and reaches an almost identical value ~0.39 $WK^{-1}m^{-1}$. The total thermal conductivity (κ) is showing a different compositional dependence as κ_L, as it increases with Pb content increasing over the entire temperature range. This might be due to the improvement of electrical conductivity upon Pb incorporation. In addition, the Pb-free sample seems to have a little bipolar effect at high temperatures.

Figure 4d indicates the values of dimensionless figure of merits (ZT), which are calculated from the values of three measured parameters α,σ and κ . The insert in Figure 4d is the ZT value against Hall carrier concentration (n_H) at 390 K, which increases with n_H value increasing. The maximum ZT value is ~0.4 at ~850 K for the sample at x=0.5, which is as high as 27 times that of pristine In_6Se_7 (ZT=0.015 @ 640 K). Although this value is still lower than those of Zn-doped α-In_2Se_3 (ZT=1.23 @ 916 K)[9] and In_4Se_3-based alloys (1.48 @ 705 K,[4] 1.40 @ 733 K,[5] 1.53 at 698 K[7]), it is 43% higher than that of Sn-substituted one (ZT= ~0.28 at 833 K),[13] and is the highest one among In_6Se_7 based alloys reported so far.

The energy gap (E_g) can be estimated using $E_g = 2\alpha_{max}eT$, where T is the temperature at which the maximum $|\alpha|$ appears, e is the electron charge and κ_B Boltzmann constant. Here it tends to reduce from 0.68 eV (~10 κ_BT at x=0.1) to 0.42 eV (~7 κ_BT at x=0.5). After $x\geq0.5$, the E_g value remains relatively constant, as shown in Figure 5a, which might be due to the reduction in carrier concentration (Figure 3a). In Figure 5a, the calculated E_g values, 0.25~0.35 eV, are displayed in color symbols, ▲, ▼, ♦, ■, upon different occupations using first principle calculation for comparison. The calculated E_g values are lower than those obtained from measurements, owing to the GGA problem.[34,35]

The significant improvement in TE performance is likely due to the enhancement of Hall carrier concentration n_H, which is caused by band structure engineering, rather than by the chemical control over carrier density via the formation of donor defect (Pb_{In}^{+}). Since there is no any deep impurity level observed within the gap upon Pb incorporation (Figure 2a-f), the annihilation centre for electrons and holes is not existent. Therefore, the enhanced thermoelectric performances suggest that the partial substitution or alloying of Pb can be used as an effective tool to tune the band structure without inducing traps for localizing the charge carriers. Such an effectiveness is somewhat analogous to that in Zintl compounds $Ca_5M_2Sb_6$ (M=Al, Ga, In).[36]

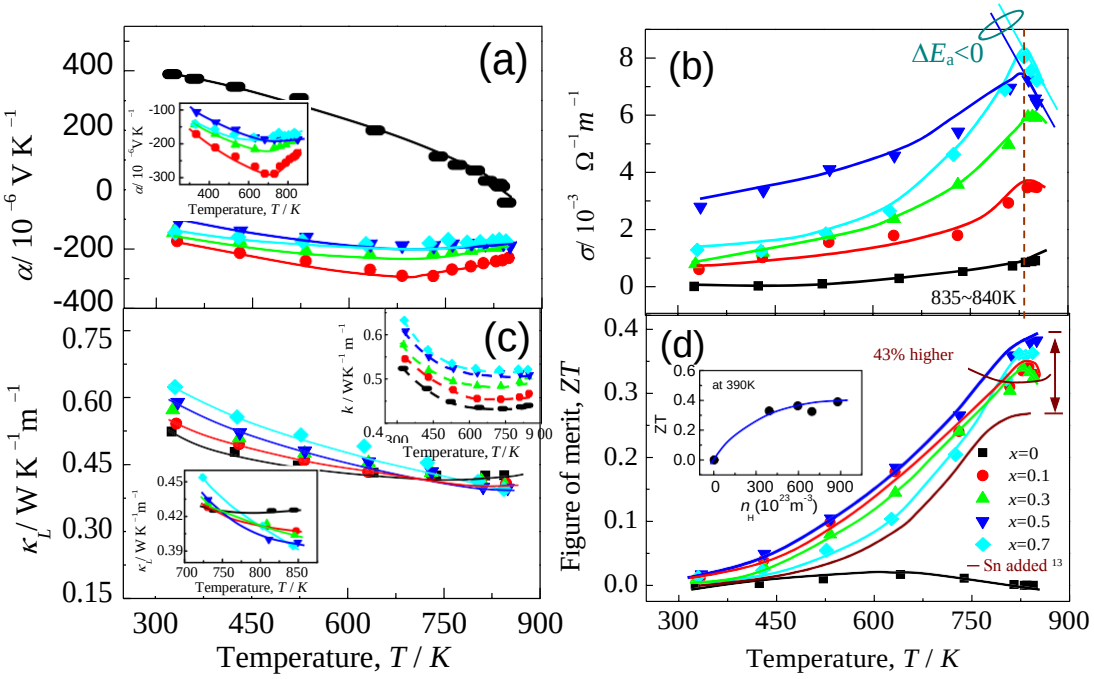

Figure 4. TE properties as function of temperature, (a) Seebeck coefficient (α), the insert is the close-up view of the α values for the Pb-incorporated samples; (b) Electrical conductivity (σ), where the thermal activation energy ΔE_a <0 as $T \geq$835~840 K for the Pb-incorporated samples; (c) lattice thermal conductivity (κ_L), where the up right inset is the total κ, and the low left one is the close-up view of the κ_L at high temperatures; (d) ZT values, the inset is the relation of ZT value with Hall carrier concentration n_H. Compared to the ZT value of Sn-added sample, the Pb-incorporated sample has a ~43% enhancement.

Similarly, the improvement in electrical conductivity upon Pb incorporation is due to the enhancement in carrier concentration, even though the estimated bandgap (E_g) is still the optimal band width in thermoelectrics.[37,38] Of course, the reduction in E_g from $10\kappa_B T$ to $7\kappa_B T$ as Pb content increases (Figure 5a) could decrease the thermal activation energy (ΔE_a) for electron excitation at high temperatures. According to the eq 3 below,

$$\sigma = \sigma_0 e^{-\Delta E_a / \kappa_B T} \qquad (3)$$

Therefore, the electrical conductivity should be increased in due course. In fact, for most Pb-incorporated samples the electrical conductivity begins to decrease with temperature elevating above 835~840K, and materials then show metallic behavior, see Figure 4b. The onset of the decreasing of the electrical conductivity at high temperatures is not observed in Sn-added samples.[13]

In order to gain a deep understanding of the band structure engineering upon Pb incorporation, the

Pisarenko plots are shown in Figure 5b, assuming m^* =0.04, 0.4 and 1.4m_e at RT and 390 K respectively. The α values for the Pb-incorporated samples at RT and 390 K decrease with n_H increasing and follow the Pisarenko plots, suggesting the dominant single parabolic band. However, from the first principle calculation (Figure 2a-f), one can see that upon Pb^{2+} occupation at the In^+ site the band tailing becomes more asymmetric with possible more tailing in conduction band as compared to valence band, and there is no any impurity level within the gap. Furthermore, the Fermi level unpins and shifts towards the conduction band, which should be resulted from the disturbance of equilibrium between the charged defects presented within the band gap, allowing the localized states conduction to be dominated. Therefore, the unpinning of the Fermi level upon Pb incorporation is directly responsible for the n-type conducting and enhancement in carrier concentration. The systematic band structures before and after Pb^{2+} incorporation are summarized in Figure 6.

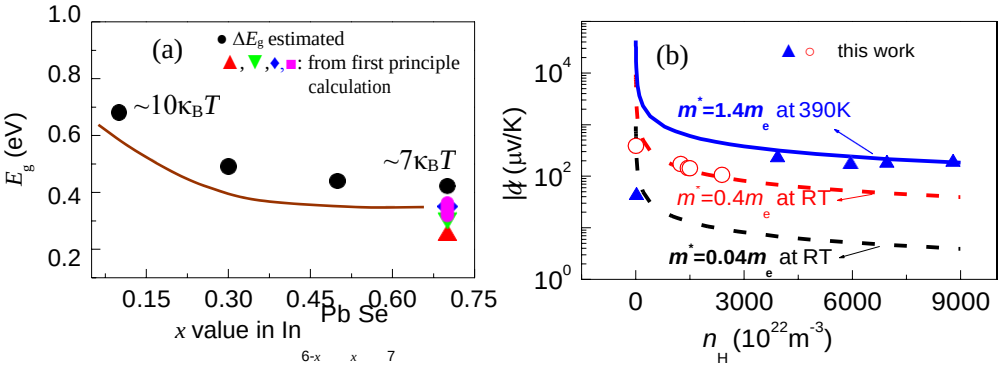

Figure 5. (a) Estimated ΔE_g values according to $\Delta E_g=2\alpha_{max}Te$, and those in color (▲,▼,♦,■) are from the first principle calculation for comparison; (b) Pisarenko plots assuming m^* =0.04, 0.4 and 1.4m_e at RT and 390 K

As Pb content increases further ($x\geq0.5$) the occupation of Pb^{2+} at In^+ site might get saturated, which allows the extra Pb^{2+} ions occupy the In^{2+} sites. In this case, F_r could move towards the valence band (Figure 2d, e), which neutralizes the effect from the occupation of Pb^{2+} at In^+ site, leading to the reduction of n_H and increasing of the mobility μ. That is the reason why we have observed the increasing tendency in mobility μ and decreasing tendency in carrier concentration n_H as Pb content increases, as shown in Figure 3a.

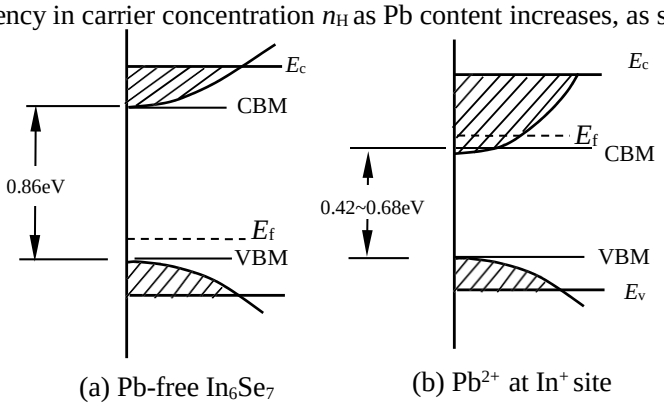

(a) Pb-free In_6Se_7 (b) Pb^{2+} at In^+ site

Figure 6. Band structure models, (a) Pb-free In_6Se_7, Fermi level (F_r) is just above the VBM; (b) When Pb^{2+} occupies In^+ site, Fermi level (F_r) lifts and gets into the conduction band (CB).

It is believed that the low carrier concentration ($8.99\times10^{22}m^{-3}$ at RT), might be the main cause to the presence of the bipolar effect in the Pb-free sample. Although the n_H values in Figure 7 are attained at 390 K, the lattice contribution (κ_L) above 390 K could still follow the carrier concentration dependence shown in

Figure 7. Since the carrier density at high Pb content shows a decreasing tendency (Figure 3a), it is anticipated that there is a decreasing tendency of phonon scattering on carriers, which is the reason why a limited reduction of κ_L is observed when Pb content, x, is higher than 0.5.

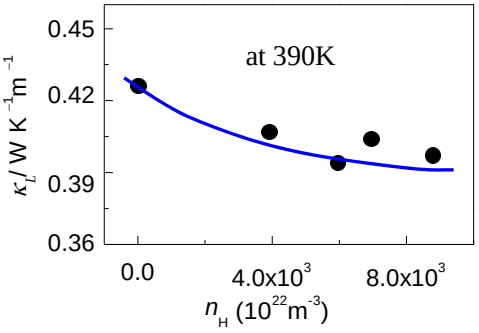

Figure 7. Lattice thermal conductivity κ_L 390K as a function of Hall carrier concentration n_H.

4. CONCLUSION

In summary, Pb-incorporated In_6Se_7 based alloys have been prepared, and their band structures and thermoelectric transport properties have been investigated. The first principle calculation reveals that Pb^{2+} prefers the In^+ to In^{3+} site, which unpins the Fermi level (E_f) and shifts it towards the conduction band. As a result, the Hall carrier concentration (n_H) has been enriched through the band structure engineering, and its value is about 2~3 orders of magnitude higher than that of intrinsic In_6Se_7. Consequently, the electrical conductivity has been improved remarkably and the TE performance has been enhanced significantly. The highest TE figure of merit (ZT) of 0.4 is attained at ~850 K, which is about 27 times that of intrinsic In_6Se_7.

Author Contributions

All authors have given approval to the final version of the paper.

Notes

The authors declare no competing financial interest.

ACKNOWLEDGMENTS

The authors thank The National Natural Science Foundation of China (Grant 51671109 and 51171084), The Zhejiang Provincial Natural Science Foundation (Grant LY14E010003 and LQ14E010001). We are also grateful to the analyses of the experimental results and first principle calculation from professor Shaoping Chen (Taiyuan University of Technology) and Dr. Z.K. Han (Shanghai Institute of Applied Physics, Chinese Academy of Sciences), respectively.

Supporting Information Available: including Crystal structure of In_6Se_7, Back-scattered SEM images for the $In_{6-x}Pb_xSe_7$ (x=0.3) bulk sample, EPMA mappings of three elements on polished $In_{6.7}Pb_{0.3}Se_7$ surface, X-ray diffraction patterns of the $In_{6-x}Pb_xSe_7$ (x=0, 0.1,0.3,0.5,0.7) powders, X-ray photoelectron spectroscopy spectra. This material is available free of charge via the Internet at http://pubs.acs.org.

REFERENCES

(1) Liu,H.; Shi,X.; Xu,F.; Zhang,L.;Zhang,W.; Chen,L.; Li,Q.; Uher,C.; Day,T.; Snyder,G.J. Copper Ion Liquid-like Thermoelectrics. *Nat. Mater*.**2012**,*11*, 422-425.

(2) Zhao,L.; Tan,G.; Hao,S.; He,J.; Pei,Y.; Chi,H.; Wang,H.; Gong,S.; Xu,H.; Dravid,V.P.; Uher,C.; Snyder,G.J.; Wolverton,C.; Kanatzidis,M.G. Ultrahigh Power Factor and Thermoelectric Performance in Hole-doped Single-crystal SnSe. *Science* **2016**,*351*,141-144.

(3) Zhao,L.; Lo,S.; Zhang,Y.; Sun,H.; Tan,G.; Uher,C.; Wolverton,C.; Dravid, V.P.; Kanatzidis,M.G. Ultralow Thermal Conductivity and High Thermoelectric Figure of Merit in SnSe crystals. *Nature* **2014**,*508*, 373-389.

(4) Rhyee,J.S.; Lee,K.H.; Lee,S.M.; Cho,E.; Kim,S. II; Lee,E.; Kwon,Y.S.; Shim,J.H.; Kotliar,G. Peierls Distortion As a Route to High Thermoelectric Performance in $In_4Se_{3-\delta}$ Crystals. *Nature* **2009**,*459*, 965-968.

(5) Lin,Z.; Chen,L.; Wang,L.; Zhao,J.; Wu,L. A Promising Mid-Temperature Thermoelectric Material Candidate: Pb/Sn-Co doped $In_4Pb_xSn_ySe_3$. *Adv.Mater.* **2013**, *25*, 4800-4806.

(6) Rhyee,J.; Ahn,K.; Lee,K.; Ji,H.; Shim,J. Enhancement of the Thermoelectric Figure-of-Merit in a Wide Temperature Range in $In_4Se_{3-x}Cl_{0.03}$ Bulk Crystals. *Adv. Mater*. **2011**, *23*, 2191-2194.

(7) Luo,Y.; Yang,J.; Li,G.; Liu,M.; Xiao,Y.; Fu,L.; Li,W.; Zhu,P.; Peng,J.; Gao,S.; Zhang,J. Enhancement of the Thermoelectric Performance of Polycrystalline $In_4Se_{2.5}$ by Copper Intercalation and Bromine Substitution. *Adv. Energy Mater*. **2014**,*4*,13005999(1-5).

(8) Han,G.; Chen,Z.; Drennan,J.; Zou,J. Indium Selenides: Structural Characteristics, Synthesis and Their Thermoelectric Performances. *Small* **2014**,*10*, 2747-2756.

(9) Cui,J.; Wang,L.; Du,Z.; Ying,P.; Deng,Y. High thermoelectric Performance of a Defect α-In_2Se_3-based Solid Solution upon Zn Substitution for In. *J. Mater. Chem. C* **2015**,*3*, 9069-9075.

(10) Walther,R.; Deiseroth,H.J. Redetermination of the Crystal Structure of Hexaindium Heptaselenide In_6Se_7. *Zeitschrift für Kristallographie* **1995**, *210*, 359.

(11) Hogg,J.H.C. The Crystal Structure of In_6Se_7. *Acta Cryst. B* **1971**,*27*,1630-1634.

(12) El-Deeb,A.F.; Metwally,H.S.; Shehata,H.A. Structural and Electrical Properties of In_6Se_7 Thin Films. *J. Phys. D: Appl.Phys.* **2008**, *41*, 125305(1-7).

(13) Cheng M.; Chen S.; Du Z.; Liu X.; Cui J. Remarkable Improvement in Thermoelectric Performance of In_6Se_7 by Substitution of Sn for In. *Phys. Status Solidi A* **2016**, DOI 10.1002/pssa.201600003

(14) Segura A.; Wünstel K.; Chevy A. Investigation of Impurity Levels in n-Type Indium Selenide by Means of Hall Effect and Deep Level Transient Spectroscopy. *Appl. Phys. A* **1983**,*31*,139-145.

(15) Gridin Vladimir,V.; Kasl,C.; Comins,J.D.; Besermana,R. Temperature Dependent Photoluminescence of the Sn-implanted InSe. *J. Appl. Phys*. **1992**,*71*, 6069-6072.

(16) Mehra,R.M.; Kohli,S.; Pundir,A.; Sachdev,V.K.; Mathur,P.C. N-Type Conduction in Pb Doped Se–In Chalcogenide Glasses. *J. Appl. Phys.* **1997**, *81*,7842-7844.

(17) Wang,L.; Ying,P.; Deng,Y.; Zhou,H.; Du,Z.; Cui,J. Site Occupations of Zn in $AgInSe_2$-based Chalcopyrites Responsible for Modified Structures and Significantly Improved Thermoelectric Performance. *RSC Adv.* **2014**,*4*,33897-33904.

(18) Yang, J.; Chen,S.; Du,Z.; Liu,X.; Cui,J. Lattice Defects and Thermoelectric Properties: The Case of P-type $CuInTe_2$ Chalcopyrite by Introduction of Zinc. *Dalton Trans.* **2014**, *43*, 15228-15236.

(19)Lukas,K.C.; Liu,W.S.; Joshi,G.; Zebarjadi,M.; Dresselhaus,M.S.; Ren,Z.F.; Chen,G.; Opeil,C.P. Experimental Determination of the Lorenz Number in $Cu_{0.01}Bi_2Te_{2.7}Se_{0.3}$ and $Bi_{0.88}$ $Sb_{0.12}$. *Phys. Rev. B* **2012**,*85*, 205410(1-5).

(20)Cui J.; Xue, H.; Xiu,W.J. Microstructures and Thermoelectric Properties of P-type Pseudo-binary

Bi-Sb-Te Alloys With Partial Substitution of Ga for Sb Prepared by Spark Plasma Sintering. *Mater. Sci. Eng. B* **2006**,*135*, 44-49.

(21)Ben Nasr,T.; Abdallah,H.B.; Bennaceur,R. First-principles Study of the Electronic and the Optical Properties of In_6Se_7 Compound. *Physica B* **2010**,*405*, 3427-3432.

(22) Li,X.; Zhang,W. Sequestration of Metal Cations with Zerovalent Iron Nanoparticles: A Study with High Resolution X-ray Photoelectron Spectroscopy (HR-XPS). *J.Phys.Chem. C* **2007**, *111*, 6939-6946.

(23) Mikhlin,Y.L.; Karacharov, A.A.; Likhatski, M.N. Effect of Adsorption of Butyl Xanthate on Galena, PbS, and HOPG Surfaces as Studied by Atomic Force Microscopy and Spectroscopy and XPS. *Int.J.Miner.Process.* **2015**,*144*,81-89.

(24) (c) Li,S.; Li,W.; Jiang,T.; Liu,Z.; Chen,X.; Cong,H.; Liu,J.; Huang,Y.; Li,L.; Huang,X. Iron Oxide with Different Crystal Phases (α- and γ‑Fe_2O_3) in Electroanalysis and Ultrasensitive and Selective Detection of Lead(II): An Advancing Approach Using XPS and EXAFS. *Anal. Chem*. **2016**, *88*, 906-914.

(25) (d) Moulder,J.F.; Chastain,J. *Handbook of X-ray Photoelectron Spectroscopy*: *A Reference Book of Standard Spectra for Identification and Interpretation of XPS Data*, Perkin-Elmer Corporation, Physical Electronics Division, Eden Prairie, Minnesota, **1992**, p.160.

(26) Snyder,G. J.; Toberer E.S. Complex Thermoelectric Materials. *Nat.Mater.* **2008**, *7*,105-114.

(27) Toberer,Eric S.; May,Andrew F.; Snyder,G.J. Zintl Chemistry for Designing High Efficiency Thermoelectric Materials. *Chem. Mater.* **2010**, *22*, 624-634.

(28)Andrew, F.M.; Fleurial,J.P.; Snyder,G. J. Optimizing Thermoelectric Efficiency in $La_{3-x}Te_4$ via Yb Substitution. *Chem. Mater.* **2010**, *22*, 2995-2999.

(29)Brown,S.R.; Toberer,E.S.; Ikeda,T.; Cox,C.A.; Gascoin,F.; Kauzlarich,S. M.; Snyder,G. J. Improved Thermoelectric Performance in $Yb_{14}Mn_{1-x}Zn_xSb_{11}$ by the Reduction of Spin-Disorder Scattering. *Chem. Mater*. **2008**, *20*, 3412-3419.

(30)Tohge,N.; Minami,T.; Tanaka,M. Electrical Transport in N-type Semiconducting $Ge_{120}Bi_xSe_{70-x}Te_{10}$ Glasses. *J.Non-Cryst. Solids* **1980**,*37*,23-30.

(31)Tohge,N.; Yonesaki T.; Minami.T. Time-of-Flight Study of Chalcogenide Glasses Chemically Modified by Bismuth. *J. Appl. Phys.* **1985**,*58*, 4225-4229.

(32)Tohge,N.; Matsuo,H.; Minami,T. Electrical Properties of N-type Semiconducting Chalcogenide Glasses in the System Pb-Ge-Se. *J. Non-Cryst. Solids* **1987**, *95* &*96*, 809-816.

(33)Kohli,S.; Sachdev,V.K.; Mehra,R.M.; Mathur,P. C. High Pressure Studies on Se-In-Pb Chalcogenide Glasses. *Phys. Stat.Sol.* (b) **1998**, *209*, 389-394.

(34)Cui,J.; Li,Y.; Du,Z.; Meng,Q.; Zhou,H. Promising Defect Thermoelectric Semiconductors $Cu_{1-x}GaSb_xTe_2$ (x=0-0.1) with Chalcopyrite Structure. *J.Mater.Chem.A* **2013**,*1*,677-683.

(35)Han,M.; Hoang,K.; Kong,H.; Pcionek,R.; Uher,C.; Paraskevopoulos,K.M.; Mahanti,S.D.; Kanatzidis,M.G. Substitution of Bi for Sb and its Role in the Thermoelectric Properties and Nanostructuring in $Ag_{1-x}Pb_{18}MTe_{20}$ (M =Bi, Sb) (x=0, 0.14, 0.3). *Chem.Mater*. **2008**, *20*, 3512-3520.

(36)Zevalkink,A.; Pomrehn,G.S.; Johnson,S.; Swallow,J.; Gibbs,Z.M. Snyder G.J. Influence of the Triel Elements (M = Al, Ga, In) on the Transport Properties of $Ca_5M_2Sb_6$ Zintl Compounds. *Chem.Mater*. **2012**, *24*, 2091-2098.

(37)Sofo,J.O.; Mahan,G.D. Optimum Band Gap of a Thermoelectric Material. *Phys.Rev.B* **1994**,*49*,4565-4570.

(38)Zhou,J.; Yang,R.; Chen,G.; Dresselhaus,M.S. Optimal Bandwidth for High Efficiency Thermoelectrics. *Phys. Rev. Lett.* **2011**,*107*, 226601(1-5).

Table of Contents/Abstract Graphic